

An Equivalent Medium Method for the Vacuum Assisted Resin Transfer Molding Process Simulation

Chensong (Jonathan) Dong *

Rakon Limited

One Pacific Rise, Mt. Wellington

Private Bag 99943, Newmarket

Auckland, New Zealand

jonathan.d@rakon.co.nz

Abstract

Computer simulation has been an efficient and cost-effective tool for the Liquid Composite Molding, including the RTM, the VARTM, and resin infusion, compared to trial-and-error. The Control Volume Finite Element Method (CVFEM) has been the predominant method for simulation. When the CVFEM simulation is used for the VARTM process, because of the existence of two distinct flow media: fiber preform and High Permeable Media (HPM), 3-D models are required. Since the HPM is usually much thinner than the fiber preform, a large number of nodes and elements need to be used in simulation, which significantly increases the computation load and time. In addition, the time-consuming pre-processing process makes simulation not feasible for industry applications.

This paper presents an Equivalent Medium Method (EMM) for fast and accurate VARTM process simulation. This method increases the thickness of the HPM or both the HPM and the fiber preform and applies the equivalent material properties. This is an improved method over previously presented Equivalent Permeability Method by correcting its two shortcomings: 1) The EPM does not account for the influence of the porosity of HPM, thus the resin flow through HPM is changed; 2) The EPM does not consider the change of through-thickness permeability after the equivalence. A new mesh generation algorithm is also discussed, which provides a faster and more convenient way for pre-processing. The approach presented in this paper provides the fundamental for developing a universal computer simulation tool for both the

* To whom all correspondence should be addressed.

RTM and VARTM processes. The effectiveness of this approach has been validated by comparing to the conventional CVFEM simulation and experiments.

Keywords: Equivalent Medium Method (EMM), Vacuum Assisted Resin Transfer Molding (VARTM), Seemann Composite Resin Infusion Molding Process (SCRIMP), High Permeable Medium (HPM), Control Volume Finite Element Method (CVFEM)

1 Introduction

The vacuum assisted resin transfer molding process (VARTM) offers many advantages over the traditional resin transfer molding such as lower tooling cost, room temperature processing. This process has been employed to manufacture many large components ranging from turbine blades and boats to rail cars and bridge decks.

In the VARTM process, parts are made by placing dry fiber reinforcing fabrics into a mold, applying a vacuum bag to the open surface and pulling a vacuum while at the same time infusing resin to saturate the fibers until the part is fully cured. This process allows for easy visual monitoring of the resin to ensure complete coverage to produce good parts without defects.

This study focuses on the Seemann Composite Resin Infusion Molding Process (SCRIMP), which was invented and patented in the late 1980's by Bill Seemann. In this VARTM process, a highly permeable distribution medium is incorporated into fiber preform as a surface layer. During infusion, resin flows preferentially across the surface and simultaneously through the preform thickness, which enables large parts to be fabricated.

The VARTM process can be divided into five steps. First, in pre-molding, the mold surface is cleaned. Then mold release agent and gel coat are sprayed onto the surface. Next, during reinforcement loading, dry fiber mats are mounted into the mold and covered by a flexible bag film. The cavity is sealed, e.g. by vacuum tapes. A vacuum is created in the mold cavity to draw the resin into the fiber mats. After the cavity is filled with resin, the resin cures and solidifies into the composite part. Finally, the solidified composite is taken out of the mold. Although this process appears simple, in actual fabrication, the procedure can be quite complicated. The locations of the inlets and outlets must be carefully selected so that the mold can be completely filled. The mold and resin temperature must be monitored to avoid resin gelling during resin infusion.

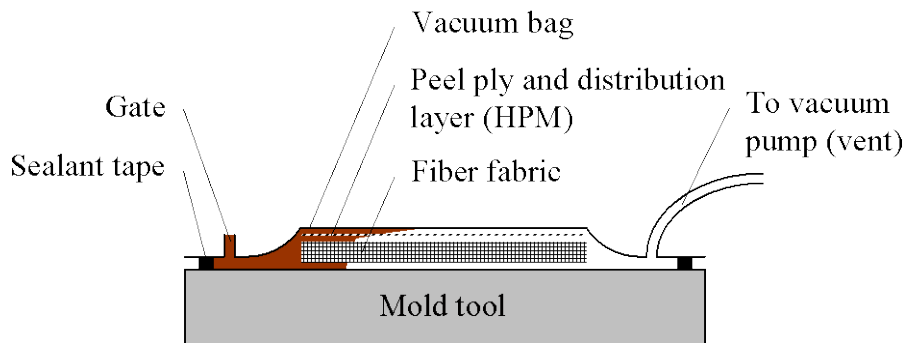


Figure 1: Vacuum assisted resin transfer molding process

Complete filling of the mold with adequate wetting of the fibrous preform is critical in the VARTM. Incomplete impregnation in the mold leads to defective parts containing dry spots. In order to achieve good quality, processing parameters such as the locations and numbers of gates and vents need to be properly set.

Traditionally, trial-and-error techniques are widely applied in the composite industry, which largely depend on the experience and skills of operators. It is very costly and time consuming. With the development of computing technology, simulation has become a powerful tool for the design and process optimization. The Control Volume Finite Element Method has been the predominant tool for simulation [1-6]. It forms and solves a set of equations for nodal control volumes as if they were finite elements. Mesh regeneration is not required, which makes the computation more efficient.

Fiber is the only flow medium in the conventional RTM process. The RTM parts are often shell-shape. Thus, the through-thickness flow can be neglected and a 2-D simulation is sufficient. The simulation is quite developed and several commercial simulation software packages are available [7-9]. In the VARTM process, there are two distinct flow media, the fiber preform and a thin layer of High Permeable Medium (HPM). The resin flow in the fiber preform has a dragging effect at the boundary of the fiber preform and HPM, which is similar to the boundary layer flow. However, the Boundary Layer Theory was developed for the case of flows for which the characteristic Reynolds number is large [10]. The resin flow in the VARTM process is a low Reynolds number laminar flow. Thus, the simulation is usually done by 3-D CVFEM. When a 3-D model is used, for large parts, the VARTM simulation requires a large

number of nodes and elements during meshing. In addition, the HPM is usually much thinner than the preform. Therefore, a finer mesh is needed to avoid high aspect ratios, which may result in difficulty in convergence and discretization error. This significantly increases the computation load and simulation time, thus, makes the simulation not feasible.

Many VARTM simulation studies have been carried out. Mathur *et al.* [11] developed an analytical model, which predicts the flow times and flow front shapes as a function of the properties of the preform, distribution media and resin. Further, they formulated a performance index to give a measure of the process efficacy. Loos *et al.* [12] developed a 3-D model to simulate the VARTM manufacturing process of complex shape composite structures. Mohan *et al.* [13] modeled and characterized the flow in channels using equivalent permeability. The equivalent permeability is used as input for numerical simulation of the mold filling process. The numerical simulations are based on a pure finite element based methodology. The mold filling in the VARTM was investigated by Sun *et al.* [14] based on a High Permeable Medium and Ni [15] *et al.* based on grooves. A 3-D Control Volume Finite Element Method was adopted to solve the flow governing equations. Based on experimental observations and CVFEM simulation, a simplified leakage flow model was presented, where they considered the preform and the peel ply as a sink for the resin, while modeling the flow in the distribution layer. Tari *et al.* [16] derived a closed form model for vacuum bag resin transfer molding under several simplifying assumptions. They assumed that the resin velocity in the saturated fiber preform is negligible. Hsiao *et al.* [17] avoided this assumption and hence the velocity for the resin, as well as the shape of the flow front through the thickness of the fiber preform, was accurately captured. Han *et al.* [18] proposed a hybrid 2.5-D and 3-D flow model.

From the literature survey, most of the studies focused on the development of simplified models due to the extensive computation involved in the 3-D CVFEM method. Currently, since RTM simulation is quite developed and has been commercialized, it is very desirable to develop a universal simulation tool incorporating both the RTM and VARTM processes. In a study previously conducted [19], an Equivalent Permeability Method was developed to incorporating two different materials, fiber and HPM. Although this method yields a very close mold filling time, it has two shortcomings: 1) The EPM does not account for the influence of the porosity of HPM, thus the resin flow through HPM is changed; 2) The EPM does not consider the change of through-thickness permeability after the equivalence. In this paper, an improved method, the

Equivalent Medium Method (EMM), is presented, which has corrected these shortcomings of the EPM and yields the same pressure distribution and flow pattern as the traditional CVFEM. The EMM can be applied not only to the HPM, but also to the fiber preform when a large part is to be simulated. The 3-D mesh information can be generated from a 2-D mesh, which makes the pre-processing process much simpler. By using this method, fewer elements are needed in the simulation. Thus, the computation time can be significantly reduced.

2 Approach

2.1 Control Volume Finite Element Method (CVFEM)

The flow of a viscous fluid through an anisotropic, homogenous, porous medium is represented by Darcy's law [20]:

$$\begin{Bmatrix} u \\ v \\ w \end{Bmatrix} = -\frac{1}{\mu} \begin{bmatrix} K_{xx} & K_{xy} & K_{xz} \\ K_{yx} & K_{yy} & K_{yz} \\ K_{zx} & K_{zy} & K_{zz} \end{bmatrix} \begin{Bmatrix} \frac{\partial p}{\partial x} \\ \frac{\partial p}{\partial y} \\ \frac{\partial p}{\partial z} \end{Bmatrix} \quad (1)$$

where K_{ij} ($i, j = x, y, \text{ or } z$) are the components of the permeability tensor. $\partial p/\partial x$, $\partial p/\partial y$ and $\partial p/\partial z$ are the pressure gradients in the three directions respectively.

For an incompressible fluid, the mass conservation equation can be reduced to the form:

$$\frac{\partial u}{\partial x} + \frac{\partial v}{\partial y} + \frac{\partial w}{\partial z} = 0. \quad (2)$$

Equation 2 can be integrated over a control volume and leads to:

$$\iiint_V \left(\frac{\partial u}{\partial x} + \frac{\partial v}{\partial y} + \frac{\partial w}{\partial z} \right) dV = 0. \quad (3)$$

Using the Divergence theorem (Gauss's theorem), the control volume integral can be transformed into a control surface integral. Thus, Equation 3 can be written as:

$$\iint_S \begin{bmatrix} n_x & n_y & n_z \end{bmatrix} \begin{Bmatrix} u \\ v \\ w \end{Bmatrix} dS = 0 \quad (4)$$

where n_x , n_y and n_z are the normal components of the surface vector of the control volume. Substituting Equation 1 into Equation 4 yields:

$$\iint_S \frac{1}{\mu} \begin{bmatrix} n_x & n_y & n_z \end{bmatrix} \begin{bmatrix} K_{xx} & K_{xy} & K_{xz} \\ K_{yx} & K_{yy} & K_{yz} \\ K_{zx} & K_{zy} & K_{zz} \end{bmatrix} \begin{Bmatrix} \frac{\partial p}{\partial x} \\ \frac{\partial p}{\partial y} \\ \frac{\partial p}{\partial z} \end{Bmatrix} dS = 0. \quad (5)$$

Equation 5 is the working equation for solving the problems of flow through anisotropic porous media and is a combination of the mass and momentum equations, while the momentum equation is represented by using the Darcy's law.

In order to solve such moving boundary problems as the resin flow front advances using the traditional finite element method, it requires the computation domain redefinition and mesh regeneration. Mesh regeneration needs a large amount of computation time as the domain becomes complicated. Alternatively, the control volume finite element method, which forms and solves a set of equations for nodal control volumes as if they were finite elements, does not require mesh regeneration. Thus, the computation is more efficient.

The control volume formation is illustrated using the three-node triangular element configuration. As shown in Figure 2, each three-node triangular element is divided into three sub-areas by connecting the centroid to the midpoints of all three sides. A control volume is composed of eight sub-areas, which have a common node at the center of the control volume.

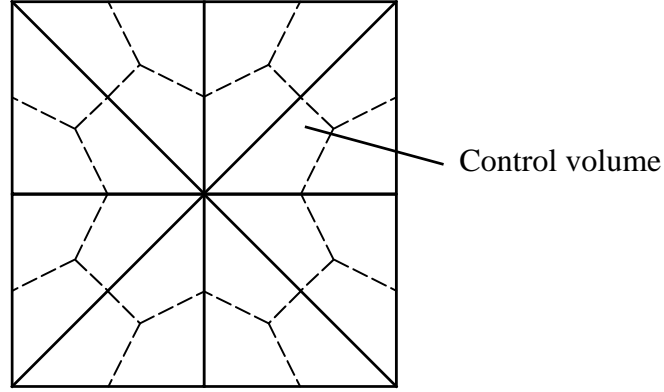


Figure 2: Control volume

The boundary conditions for mold filling simulation are as follows:

At the flow front:

$$p = 0. \quad (6)$$

At the inlet gates:

$$\text{For constant pressure: } p = p_0; \quad (7)$$

$$\text{For the constant flow rate: } \mathbf{v} = \mathbf{v}_0. \quad (8)$$

At the mold boundaries:

$$\frac{\partial p}{\partial \mathbf{n}} = 0. \quad (9)$$

At the flow front, a parameter f is used to represent the status of each control volume in the flow domain. If the control volume has not been occupied by the fluid, f is equal to zero. If the control volume is partially filled, f is equal to the volume fraction of the fluid occupying the control volume. f factor is set to 1 if the volume is completely filled by advancing fluid. The control volumes with f values varying between 0 and 1 are considered flow front elements. The pressure in these partially filled flow front control volumes is set to the ambient pressure. With the aforementioned boundary conditions, the set of linear algebraic equations can be solved to determine the pressure field at each time step during mold filling. Based on the calculated pressure field, the velocity field can then be computed using Darcy's law.

2.2 RTM and VARTM Simulation

In the traditional RTM process, fiber preform is the only flow medium. The through-thickness resin flow can often be neglected and thus a 2D model can be applied, as shown in Figure 3.

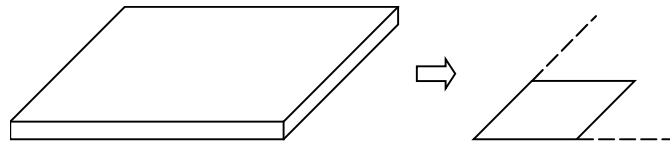


Figure 3: 2-D CVFEM model for RTM process

In the VARTM process, however, another flow medium, High Permeable Medium (HPM), presents. Considering a 1-D flow in the VARTM process, the resin flow front is plotted in Figure 4. The HPM is much thinner than the preform. The flow is assumed to be well developed and can be divided into two regions: saturated region and flow front region.

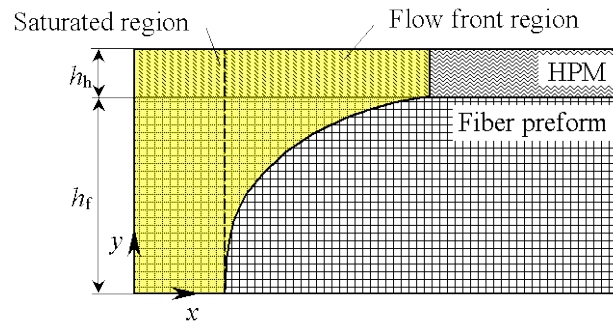


Figure 4: Resin flow in VARTM process

A general rule of thumb in FEA is to avoid high aspect ratios. High aspect ratios often lead to problems and difficulty in convergence. In this 3-D VARTM simulation, since the HPM is much thinner than the fiber preform, a large number of elements are needed to satisfy the required robustness in numerical computation, as shown in Figure 5. This, in turn, tremendously increases computation time. To overcome this shortcoming, the most convenient way is to

increase the thickness of HPM to match that of the fiber preform. Thus, fewer elements are needed. After the thickness increment of the HPM, its material properties need to be modified to yield the same pressure distribution and flow pattern. This introduces the concept of the Equivalent Medium Method (EMM).

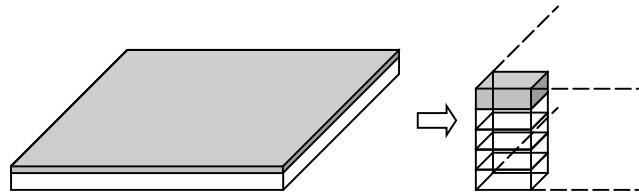


Figure 5: 3-D CVFEM model for VARTM process

2.3 Equivalent Medium Method

The concept of the EMM is shown in Figure 6. When the 3-D mesh is generated, the thickness of the HPM is increased to that of the fiber preform. The material properties need to be modified to accommodate this increase. The modified material properties are used in the simulation. Since the thickness of the HPM is equal to that of the fiber preform, fewer elements are needed than in the traditional CVFEM.

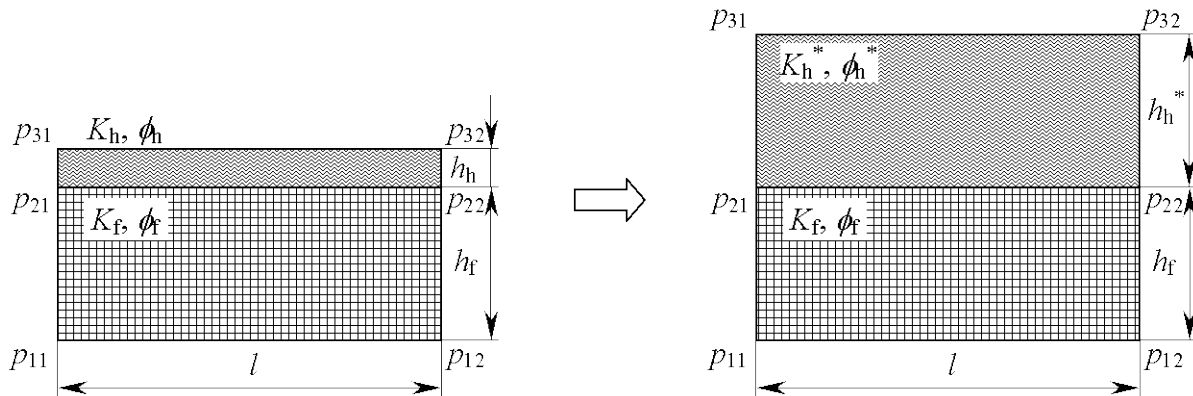


Figure 6: Equivalent Medium Method (EMM)

Generally, the material properties relevant to flow are the porosity ϕ , the in-plane permeability K_{11} , K_{22} , and the through-thickness permeability K_{33} .

First, the porosity of the equivalent HPM is derived. After the thickening of the HPM, the flow velocity and mass flow should be the same. Thus,

$$u^* = u. \quad (10)$$

$$u^* h_h^* \phi_h^* = u h_h \phi_h. \quad (11)$$

From Equations 10 and 11, the porosity of the equivalent HPM is

$$\phi_h^* = \phi_h \frac{h_h}{h_h^*}. \quad (12)$$

After the equivalent porosity is derived, the equivalent in-plane permeability K_{11} and K_{22} is derived. From the Darcy's law,

$$\phi_h^* u^* = -\frac{K_{11h}^*}{\mu} \cdot \frac{dp^*}{dx}, \quad (13a)$$

$$\phi_h u = -\frac{K_{11h}}{\mu} \cdot \frac{dp}{dx}. \quad (13b)$$

Since the pressure field should be the same after the thickening of the HPM, i.e. $dp^*/dx = dp/dx$, the in-plane permeability of the equivalent HPM can be derived as

$$K_{11h}^* = K_{11h} \cdot \frac{h_h}{h_h^*}. \quad (14a)$$

Likewise,

$$K_{22h}^* = K_{22h} \cdot \frac{h_h}{h_h^*}. \quad (14b)$$

Last, the equivalent through-thickness permeability K_{33} is derived. After the thickening of the HPM, the through-thickness flow velocity should be the same. Thus,

$$w^* = h_h^*/t, \quad (15a)$$

$$w = h_h/t. \quad (15b)$$

i.e.

$$\frac{w^*}{w} = \frac{h_h^*}{h_h}. \quad (16)$$

From the Darcy's law,

$$w^* = \frac{K_{33h}^* \Delta p}{\phi_h^* h_h^*}, \quad (17a)$$

$$w = \frac{K_{33h} \Delta p}{\phi_h h_h}. \quad (17b)$$

Substituting Equation 12 into 17 yields

$$\frac{w^*}{w} = \frac{K_{33h}^*}{K_{33h}}. \quad (18)$$

Substituting Equation 16 into 18 yields,

$$K_{33h}^* = K_{33h} \cdot \frac{h_h^*}{h_h}. \quad (19)$$

In some situation, when a large part is to be simulated, both the HPM and the fiber preform can be thickened to reduce the number of elements and maintain good aspect ratios.

As shown in Equation 1, permeability of fiber is represented as a tensor. The components of the tensor are defined in a 3-D Cartesian coordinate system. Since the permeability values of a fiber mat are usually defined in its principal directions, an important issue is to relate the material coordinate system to the global coordinate system.

As shown in Figure 7, the principal directions of a fiber mat compose the material coordinate system 1-2-3. The permeability values in the material coordinate system can be transformed to the global coordinate system by

$$\begin{bmatrix} K_{xx} & K_{xy} & K_{xz} \\ K_{yx} & K_{yy} & K_{yz} \\ K_{zx} & K_{zy} & K_{zz} \end{bmatrix} = \begin{bmatrix} l_{11} & l_{12} & l_{13} \\ l_{21} & l_{22} & l_{23} \\ l_{31} & l_{32} & l_{33} \end{bmatrix} \begin{bmatrix} K_{11} & 0 & 0 \\ 0 & K_{22} & 0 \\ 0 & 0 & K_{33} \end{bmatrix} \begin{bmatrix} l_{11} & l_{21} & l_{31} \\ l_{12} & l_{22} & l_{32} \\ l_{13} & l_{23} & l_{33} \end{bmatrix} \quad (20)$$

where l_{ij} is the directional cosine of local coordinate x , y , and z with respect to the principal axes 1, 2, 3; K_{11} , K_{22} , and K_{33} are the permeability of the fiber mat in three principal directions.

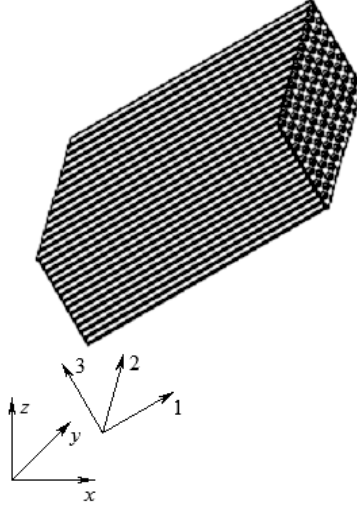


Figure 7: Principal directions of a fiber mat in the global coordinate system

In order to relate the material coordinate system to the global coordinate system, two vectors \mathbf{u}_1 and \mathbf{u}_2 are defined, where \mathbf{u}_1 and \mathbf{u}_2 are the unit vector of principal axes 1 and 2 in the global coordinate system, $\mathbf{u}_3 = \mathbf{u}_1 \times \mathbf{u}_2$. Thus, the permeability can be defined in three principal directions and the directional cosines can be derived based on \mathbf{u}_1 and \mathbf{u}_2 .

The equivalent permeability can be derived in the principal directions first and converted to the permeability tensor in the global coordinate system by using Equation 20.

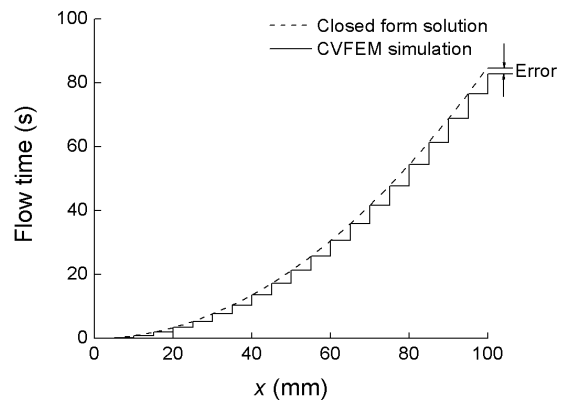
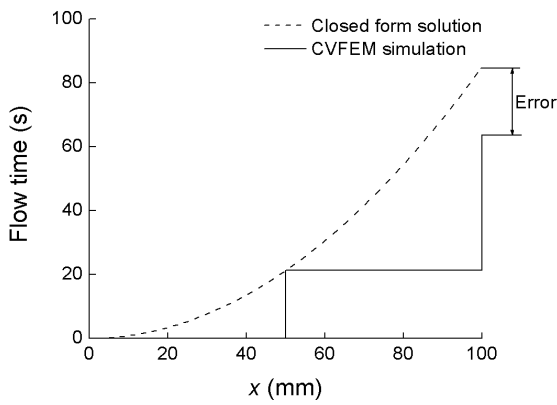
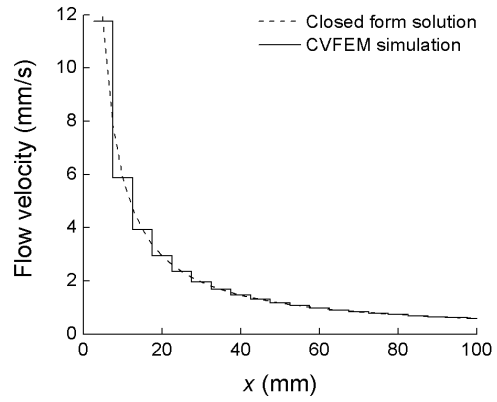
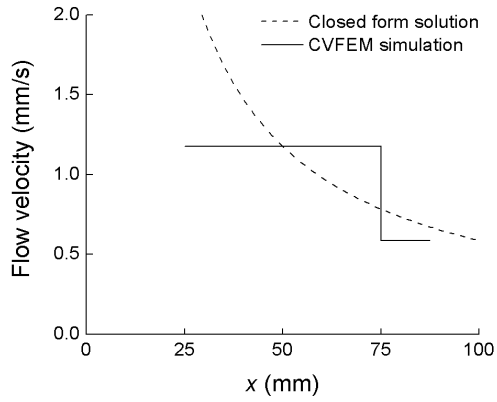
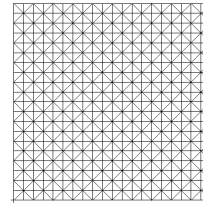
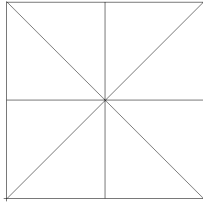
2.4 Considerations in Mesh Generation

A general issue in the CVFEM based mold filling simulation is mesh generation, including both the RTM and the VARTM simulation. Generally, a finer mesh yields a more accurate simulation result but significantly increases simulation time. In order to obtain a general rule of thumb for meshing to achieve the accuracy requirement and time efficiency, a 1-D RTM mold filling simulation using different mesh density was studied since the closed form solution could be easily found by

$$t_{fill} = \frac{\mu l^2}{2Kp_0}, \quad (21)$$

where t_{fill} is the mold filling time and l is the 1-D flow distance.

The part being simulated is a flat square panel of 100 mm×100 mm. Linear injection at 1×10^5 MPa was assumed. The viscosity is 200 cP. The permeability of fiber is 60 darcy and the porosity is 51%. The mold filling processes using two different mesh densities (8 and 800 elements) are shown in Figure 8, along with the closed form solution. The mold filling time is plotted vs. the number of mesh seeds in Figure 9, along with the closed form solution and relative error. It concludes that as a general rule of thumb, in order to control the relative error within 5%, the number of mesh seeds should be at least 20. This can be applied to both the RTM and the VARTM simulation.



a) Number of mesh seeds = 2; 8 elements b) Number of mesh seeds = 20; 800 elements

Figure 8: Influence of mesh density on mold filling process

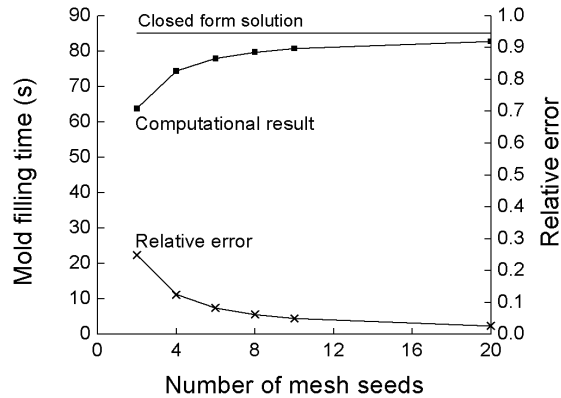


Figure 9: Influence of mesh density on mold filling time

2.5 Mesh Generation Algorithm

An issue in applying the VARTM simulation is 3-D mesh generation. Traditionally, when a different HPM or fiber preform is used, the pre-processing process needs to be repeated, which includes building a new CAD model and meshing. This is not convenient for the composite product and process design optimization. Thus, it is necessary to develop an algorithm to avoid such repeated pre-processing process.

If the thickness of the HPM and the fiber preform is known, the 3-D mesh information can be obtained from geometry calculations. Thus, if an algorithm converting 2-D meshes to 3-D is developed, only a one-time 2-D CAD model and mesh need to be created. In this way, users can try several options of HPM and fiber preforms without going through the repetitive preprocessing process. A comparison between these two methods is shown in Figure 10. An example of 3-D mesh generation from 2-D is shown in Figure 11.

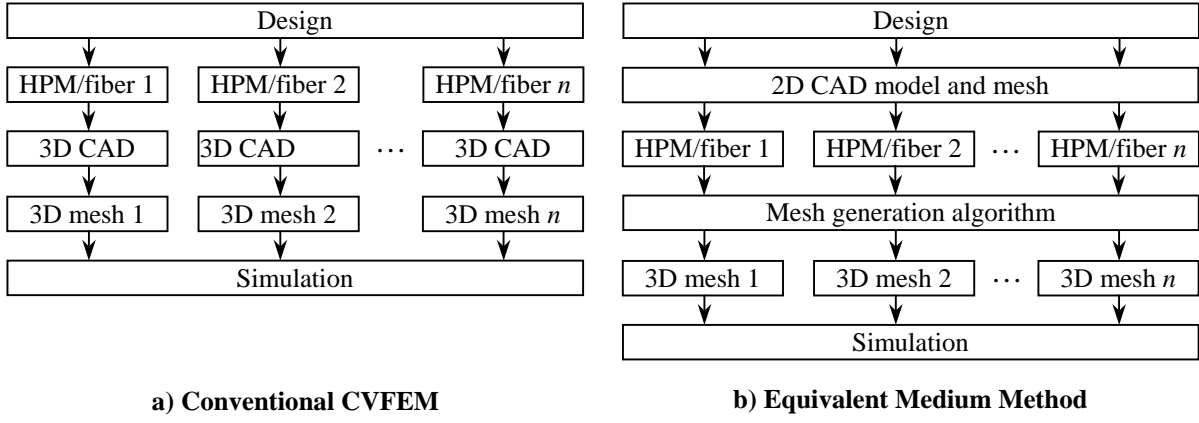


Figure 10: Comparison of the conventional CVFEM and the Equivalent Method on the simulation process

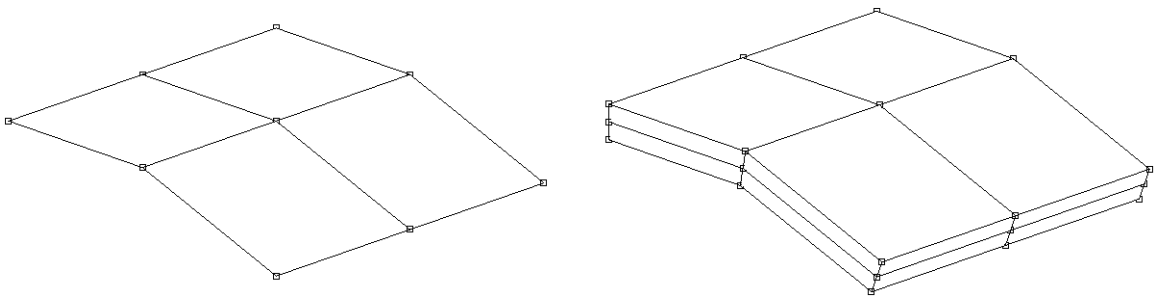


Figure 11: 3D mesh generation from 2D mesh

The algorithm is illustrated by a 1-D example. As shown in Figure 12, the line elements $\overline{\mathbf{P}_1\mathbf{P}_2}$ and $\overline{\mathbf{P}_2\mathbf{P}_3}$ are expanded into 2-D elements $\mathbf{P}_1\mathbf{P}_2\mathbf{P}_5\mathbf{P}_4$, etc of thickness h , which is defined by users. The problem can now be regarded as given the coordinates of \mathbf{P}_1 to \mathbf{P}_3 as (x_1, y_1) , (x_2, y_2) , and (x_3, y_3) , find the coordinates of \mathbf{P}_4 to \mathbf{P}_9 .

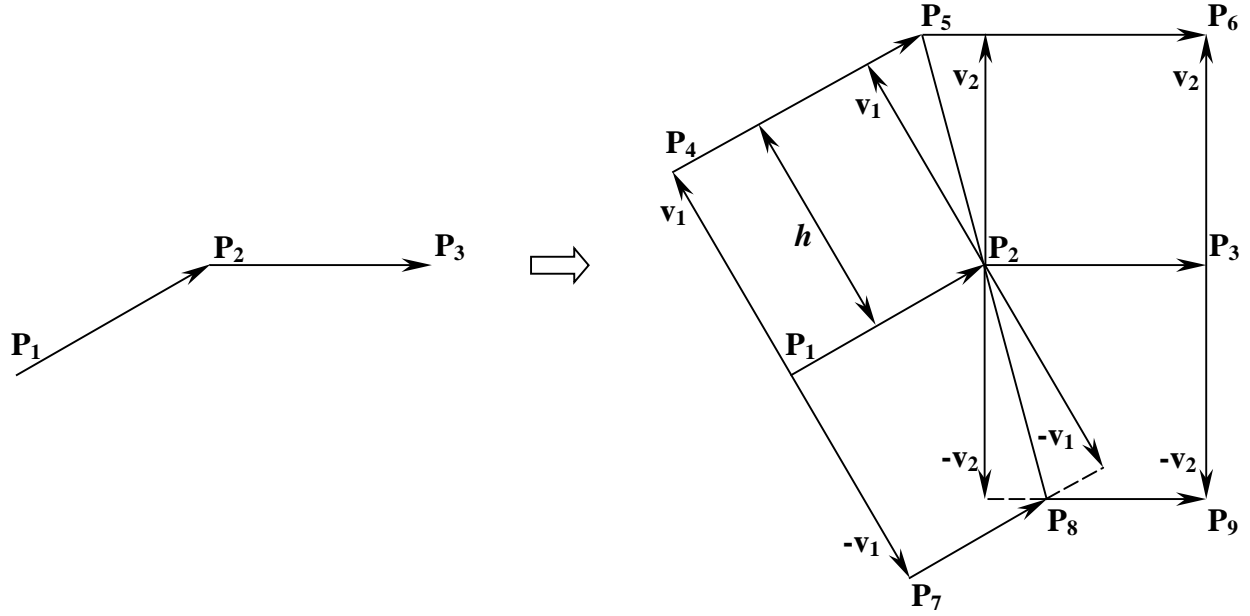


Figure 12: Mesh generation algorithm

The 1-D elements can be regarded as a series of vectors whose directions are determined by the mesh connectivity information, i.e.

$$\mathbf{P}_1\mathbf{P}_2 = \begin{Bmatrix} x_2 - x_1 \\ y_2 - y_1 \end{Bmatrix}, \quad \mathbf{P}_2\mathbf{P}_3 = \begin{Bmatrix} x_3 - x_2 \\ y_3 - y_2 \end{Bmatrix}.$$

The normal vector can be expressed as

$$\mathbf{v}_1 = \begin{Bmatrix} -\frac{h(y_2 - y_1)}{\sqrt{(x_2 - x_1)^2 + (y_2 - y_1)^2}} \\ \frac{h(x_2 - x_1)}{\sqrt{(x_2 - x_1)^2 + (y_2 - y_1)^2}} \end{Bmatrix}, \quad (22a)$$

$$\mathbf{v}_2 = \begin{Bmatrix} -\frac{h(y_3 - y_2)}{\sqrt{(x_3 - x_2)^2 + (y_3 - y_2)^2}} \\ \frac{h(x_3 - x_2)}{\sqrt{(x_3 - x_2)^2 + (y_3 - y_2)^2}} \end{Bmatrix}. \quad (22b)$$

The coordinates of points \mathbf{P}_4 , \mathbf{P}_6 , \mathbf{P}_7 , and \mathbf{P}_9 can be simply derived as

$$\begin{cases} x_4 \\ y_4 \end{cases} = \begin{cases} x_1 - h \frac{y_2 - y_1}{\sqrt{(x_2 - x_1)^2 + (y_2 - y_1)^2}} \\ y_1 + h \frac{x_2 - x_1}{\sqrt{(x_2 - x_1)^2 + (y_2 - y_1)^2}} \end{cases}, \quad (23)$$

$$\begin{cases} x_6 \\ y_6 \end{cases} = \begin{cases} x_3 - h \frac{y_3 - y_2}{\sqrt{(x_3 - x_2)^2 + (y_3 - y_2)^2}} \\ y_3 + h \frac{x_3 - x_2}{\sqrt{(x_3 - x_2)^2 + (y_3 - y_2)^2}} \end{cases}, \quad (24)$$

$$\begin{cases} x_7 \\ y_7 \end{cases} = \begin{cases} x_1 + h \frac{y_2 - y_1}{\sqrt{(x_2 - x_1)^2 + (y_2 - y_1)^2}} \\ y_1 - h \frac{x_2 - x_1}{\sqrt{(x_2 - x_1)^2 + (y_2 - y_1)^2}} \end{cases}, \quad (25)$$

$$\begin{cases} x_9 \\ y_9 \end{cases} = \begin{cases} x_3 + h \frac{y_3 - y_2}{\sqrt{(x_3 - x_2)^2 + (y_3 - y_2)^2}} \\ y_3 - h \frac{x_3 - x_2}{\sqrt{(x_3 - x_2)^2 + (y_3 - y_2)^2}} \end{cases}. \quad (26)$$

The coordinates of points \mathbf{P}_5 and \mathbf{P}_8 are more complex. \mathbf{P}_5 can be regarded as the intersection of line $\overline{\mathbf{P}_4\mathbf{P}_5}$ and line $\overline{\mathbf{P}_5\mathbf{P}_6}$. The equation of line $\overline{\mathbf{P}_4\mathbf{P}_5}$ can be expressed as

$$y - \left[y_2 + h \frac{x_2 - x_1}{\sqrt{(x_2 - x_1)^2 + (y_2 - y_1)^2}} \right] = \frac{y_2 - y_1}{x_2 - x_1} \left\{ x - \left[x_2 - h \frac{y_2 - y_1}{\sqrt{(x_2 - x_1)^2 + (y_2 - y_1)^2}} \right] \right\},$$

i.e.

$$(y_2 - y_1)x - (x_2 - x_1)y = (x_1y_2 - x_2y_1) - h\sqrt{(x_2 - x_1)^2 + (y_2 - y_1)^2}. \quad (27)$$

Likewise, the equation of line $\overline{\mathbf{P}_5\mathbf{P}_6}$ can be expressed as

$$(y_3 - y_2)x - (x_3 - x_2)y = (x_2y_3 - x_3y_2) - h\sqrt{(x_3 - x_2)^2 + (y_3 - y_2)^2}. \quad (28)$$

By solving Equations 27 and 28, the coordinates of \mathbf{P}_5 are

$$\begin{cases} x_5 \\ y_5 \end{cases} = \begin{cases} x_2 + \frac{h \left[(x_3 - x_2) \sqrt{(x_2 - x_1)^2 + (y_2 - y_1)^2} - (x_2 - x_1) \sqrt{(x_3 - x_2)^2 + (y_3 - y_2)^2} \right]}{x_1 y_2 - x_2 y_1 + x_2 y_3 - x_3 y_2 + x_3 y_1 - x_1 y_3} \\ y_2 + \frac{h \left[(y_3 - y_2) \sqrt{(x_2 - x_1)^2 + (y_2 - y_1)^2} - (y_2 - y_1) \sqrt{(x_3 - x_2)^2 + (y_3 - y_2)^2} \right]}{x_1 y_2 - x_2 y_1 + x_2 y_3 - x_3 y_2 + x_3 y_1 - x_1 y_3} \end{cases} \quad (29)$$

Likewise, the coordinates of \mathbf{P}_8 are

$$\begin{cases} x_8 \\ y_8 \end{cases} = \begin{cases} x_2 - \frac{h \left[(x_3 - x_2) \sqrt{(x_2 - x_1)^2 + (y_2 - y_1)^2} - (x_2 - x_1) \sqrt{(x_3 - x_2)^2 + (y_3 - y_2)^2} \right]}{x_1 y_2 - x_2 y_1 + x_2 y_3 - x_3 y_2 + x_3 y_1 - x_1 y_3} \\ y_2 - \frac{h \left[(y_3 - y_2) \sqrt{(x_2 - x_1)^2 + (y_2 - y_1)^2} - (y_2 - y_1) \sqrt{(x_3 - x_2)^2 + (y_3 - y_2)^2} \right]}{x_1 y_2 - x_2 y_1 + x_2 y_3 - x_3 y_2 + x_3 y_1 - x_1 y_3} \end{cases} \quad (30)$$

3 Model Validation

First, the VARTM processing of a simple flat panel was simulated. The dimensions of the flat panel, as shown in Figure 13, are 100 mm×100 mm×4 mm. The material properties are shown in Table 1. The single port injection method was used.

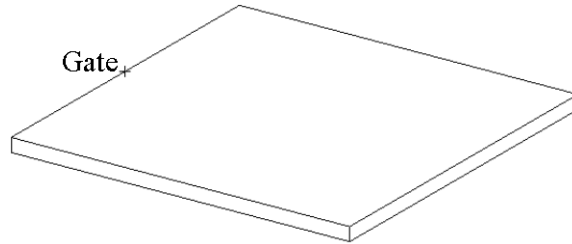


Figure 13: A flat panel

Table 1: Material properties of flat panel

	h (mm)	ϕ	K_{11} (darcy)	K_{33} (darcy)
Fiber	4	0.5	100	20
HPM	1	0.8	3000	3000

Half of the structure was modeled due to symmetry. The resin was injected into the mold cavity at full vacuum and its viscosity was 200 cP.

When the traditional method was used, five elements were used in the thickness direction to achieve good aspect ratio because of the big difference in thickness between the fiber preform and the HPM. When the EMM was used, the thickness of the HPM was increased to 4 mm and only two elements were needed in the thickness direction. The mesh is shown in Figure 14. The equivalent material properties of the HPM were computed as: $\phi_h^* = 0.2$; $K_{11h}^* = 750$ darcy and $K_{33h}^* = 12000$ darcy.

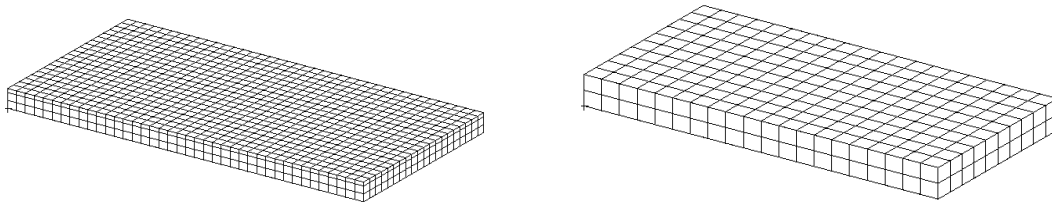


Figure 14: Mesh of flat panel
Left: traditional method; right: Equivalent Medium Method

The simulation results by the traditional method and the EMM are shown in Table 2 and Figure 15. It shows that the EMM yields a comparable accuracy (Relative error = 15.6%) while achieving a computation time saving of 93.2%.

Table 2: Filling time of flat panel

	Number of nodes	Number of elements	Computation time	Mold filling time (s)
Traditional method	3444	2400	1h20'19"	30.1
Equivalent Medium Method	693	400	5'28"	25.4

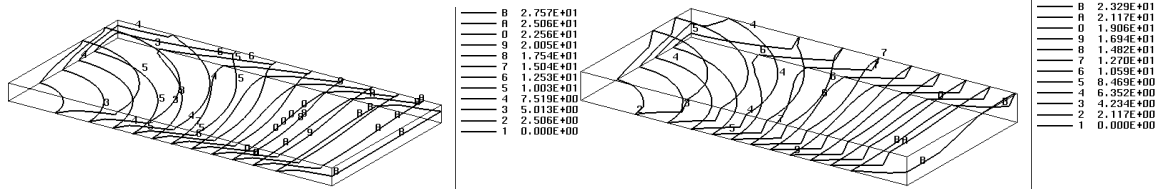


Figure 15: Mold filling process of flat panel

Left: traditional method; right: Equivalent Medium Method

Next, validations were further conducted against the results from Reference [15]. As shown in Figure 16, the length and width of the fiber mat are 640 mm and 110 mm, respectively. The single port injection method was used. Half of the structure was modeled due to symmetry. The injection pressure was at constant full vacuum pressure.

When the EMM was used, the same mesh was used for all the four cases. Thus, the thicknesses of both the fiber preform and the HPM were increased in cases 1-3, and only the thickness of the HPM was increased in case 4, as shown in Tables 3 and 4, along with the original and equivalent material properties.

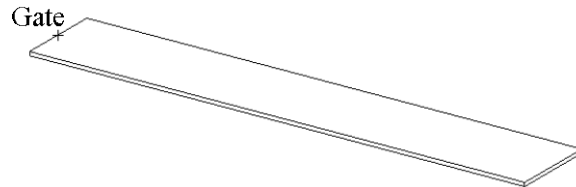


Figure 16: Test part in reference [14]

Table 3: Material properties of fiber preform

Case	Number of fiber mats	h_f (mm)	ϕ_f	K_{11f} (darcy)	K_{33f} (darcy)	h_f^* (mm)	ϕ_f^*	K_{11f}^* (darcy)	K_{33f}^* (darcy)
1	2	4	0.49	60	10	12	0.163	20	30
2	3	6	0.49	60	10	12	0.245	30	20
3	4	8	0.49	60	10	12	0.327	40	15
4	6	12	0.49	60	10	12	0.490	60	10

Table 4: Material properties of HPM

Case	h_h (mm)	ϕ_h	K_{11h} (darcy)	K_{33h} (darcy)	h_h^* (mm)	ϕ_h^*	K_{11h}^* (darcy)	K_{33h}^* (darcy)
1-4	0.8	0.85	2800	2800	12	0.057	186.667	42000

Figures 17 and 18 show the flow fronts simulated by using the traditional method and the EMM for case 1 and 4, respectively. The complete simulation results using the traditional method, the EMM and the leakage model [14], along with the experimental results [14] are shown in Table 5 and plotted in Figure 19.

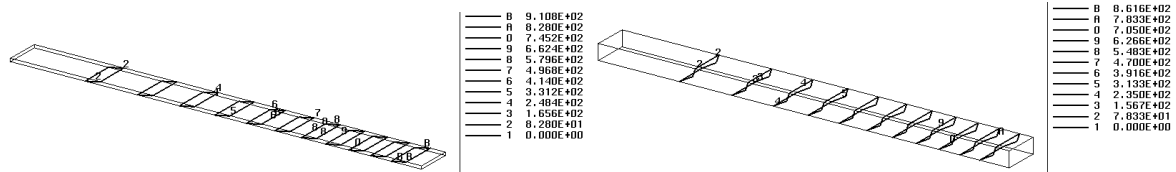


Figure 17: Mold filling process of case 1

Left: traditional method; right: Equivalent Medium Method

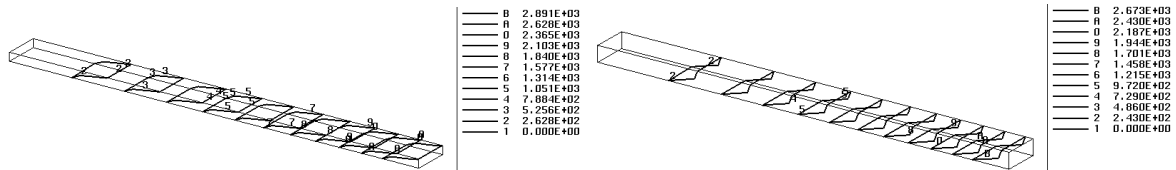


Figure 18: Mold filling process of case 4

Left: traditional method; right: Equivalent Medium Method

Table 5: Simulation and experimental results

Case	Viscosity (cP)/ Room temp (°C)	Mold filling time (s)			Experiment
		Traditional method	EMM	Leakage model	
1	325/26.0	994	940	728	807
2	325/26.0	1312	1238	942	960
3	430/21.7	2142	1996	1509	1680
4	470/20.5	3154	2916	2157	2340

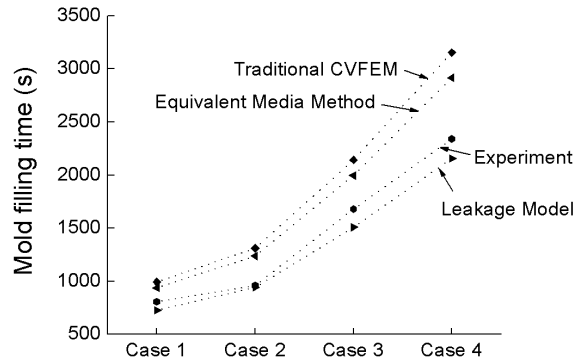


Figure 19: Comparison of EMM with traditional CVFEM, leakage model, and experimental results

Conclusions are drawn from Table 5 and Figure 19 that the simulation result from the EMM agrees very well with that from the traditional method. Both the traditional method and the EMM yield a longer mold filling time than the experiments, which may be caused by the racetracking phenomenon not included in modeling. The leakage model gives a shorter mold filling time. The Equivalent Medium Method is capable of simulating the mold filling process with acceptable accuracy.

4 Case Study – Cover Plate of UAV

As a case study, the cover plate of an Unmanned Aerial Vehicle (UAV) made by the VARTM process, as shown in Figure 20, was simulated by both the traditional method and the Equivalent Medium Method. The approximate dimensions are: length: 840 mm; width: 281 mm; height: 137 mm.

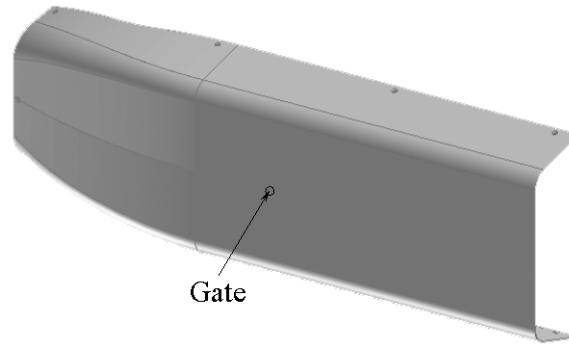


Figure 20: Cover plate of Unmanned Aerial Vehicle (UAV)

Half of the structure was modeled due to symmetry. The mold filling process was simulated by traditional method and the EMM respectively. The mesh is shown in Figure 21. The traditional method used 5940 elements while the EMM used only 660 elements. The original and equivalent material properties are shown in Table 6.

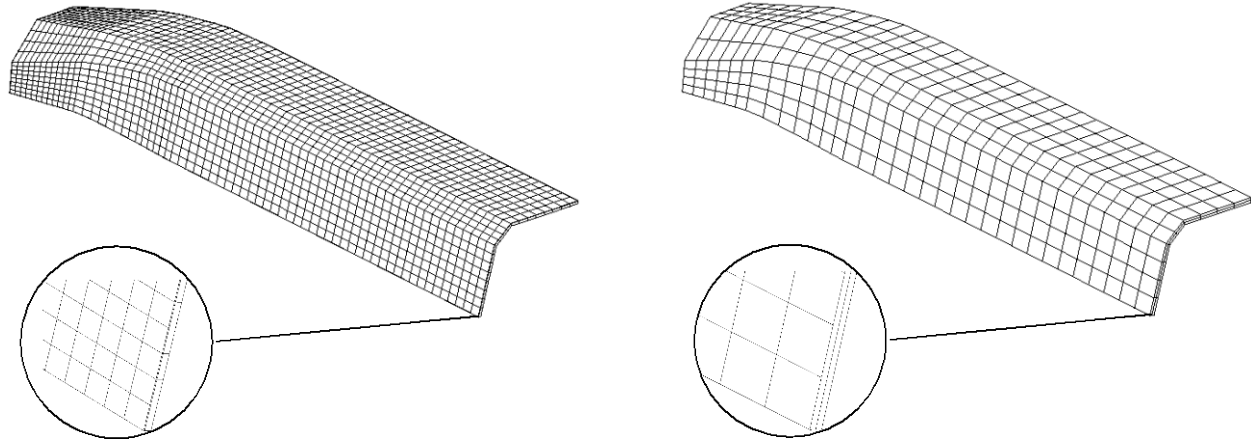


Figure 21: Mesh of cover plate

Left: traditional method; right: Equivalent Medium Method

Table 6: Material properties of cover plate

	h (mm)	ϕ	K_{11} (darcy)	K_{33} (darcy)	h^* (mm)	ϕ^*	K_{11} (darcy)	K_{33} (darcy)
Fiber	3	0.50	60	10	3.0	0.50	60	10
HPM	0.5	0.85	2800	2800	3.0	0.14	466.67	16800

The simulation results are shown in Figure 22. The mold filling time by the original simulation method is 708 sec and the computation time is 6h38'35". The mold filling time by the EMM is 600 sec and the computation time was reduced to 52'23". The difference of mold filling time is 15% while the time saving is 87%.

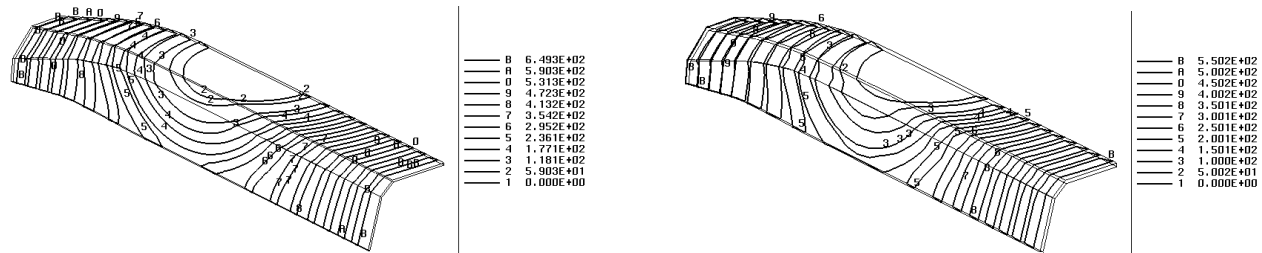


Figure 22: Mold filling process of cover plate

Left: traditional method; right: Equivalent Medium Method

5 Conclusions

Computer simulation has been an efficient and cost-effective tool for the Liquid Composite Molding, including the RTM, the VARTM, and resin infusion, compared to trial-and-error. The Control Volume Finite Element Method (CVFEM) has been the predominant method for simulation. When the CVFEM simulation is used for the VARTM process, because of the existence of two distinct flow media: fiber preform and High Permeable Media (HPM), 3-D models are required. Since the HPM is usually much thinner than the fiber preform, a large number of nodes and elements need to be used in simulation, which significantly increases the computation load and time. In addition, the time-consuming pre-processing process makes simulation not feasible for industry applications.

This paper presents an Equivalent Medium Method (EMM) for fast and accurate VARTM process simulation. This method increases the thickness of the HPM or both the HPM and the fiber preform and applies the equivalent material properties. This is an improved method over previously presented Equivalent Permeability Method [19] by correcting its two shortcomings: 1) The EPM does not account for the influence of the porosity of HPM, thus the resin flow through HPM is changed; 2) The EPM does not consider the change of through-thickness permeability after the equivalence. When the EMM is used in simulation, since fewer

nodes and elements are required to ensure good aspect ratios, the computation load is reduced significantly. The effectiveness of this approach has been validated by comparing to the conventional CVFEM simulation and experiments. It shows that the simulation time can be reduced by more than 85% while maintaining a comparable accuracy. The pre-processing algorithm discussed provides a faster and more convenient way for mesh generation. The approach presented in this paper provides the fundamental for developing a universal computer simulation tool for both the RTM and VARTM processes.

References

- [1] Brusckhe, M.V. and Advani, S.G. (1991). Filling Simulation of Complex Three-Dimensional Shell-Like Structures, *SAMPE Quarterly*, 23(1): 2-11.
- [2] Young, W.B., Han, K., Fong, L.H. and Lee, L.J. (1991). Flow Simulation in Molds with Preplaced Fiber Mats, *Polymer Composites*, 12(6): 391-404.
- [3] Liu, X.L. (2000). Isothermal Flow Simulation of Liquid Composite Molding, *Composites Part A*, 31(12): 1295-1302.
- [4] Lin, R.J., Lee, L.J. and Liou, M.J. (1991). Non-Isothermal Mold Filling and Curing Simulation in Thin Cavities with Preplaced Fiber Mats, *International Polymer Processing*, VI(4): 356-369.
- [5] Young, W.B., "Three-Dimensional Nonisothermal Mold Filling Simulation in Resin Transfer Molding," *Polymer Composites*, 15(2): 118-127 (1994).
- [6] Lee, L.J., Young, W.B. and Lin, R.J. (1994). Mold Filling and Curing Modeling of RTM and SCRIM Processes, *Composite Structures*, 27(1-2): 109-120.
- [7] LIMS, Center for Composite Materials, University of Delaware, www.ccm.udel.edu/Research/AMIPCindex.html.
- [8] PAM-RTM, ESI Group, www.esi-group.com.
- [9] Polyworx, www.polyworx.com.
- [10] Cowley S.J. (2001). Laminar Boundary-Layer Theory: A 20th Century Paradox?, in *Mechanics for a New Millennium: Proceedings of the 20th International Congress of*

Theoretical and Applied Mechanics, Chicago, Illinois, USA, 27 August-2 September 2000, eds. H. Aref and J.W. Phillips, Kluwer Academic Publishers, Dordrecht, the Netherlands, 389-411.

- [11] Mathur, R., Heider, D., Hoffmann, C., Gillespie, J.W.Jr., Advani, S.G. and Fink, B.K. (2001). Flow Front Measurements and Model Validation in the Vacuum Assisted Resin Transfer Molding Process, *Polymer Composites*, 22(4): 477-490.
- [12] Loos, A.C., Sayre, J., McGrane, R. and Grimsley, B. (2001). VARTM Process Model Development, in *Proceedings of the 46th International SAMPE Symposium, Long Beach, CA, USA*, SAMPE Publishing, 46(I): 1049-1061.
- [13] Mohan, R.V., Shires, D.R., Tamma, K.K. and Ngo, N.D. (1998). Flow Channels/Fiber Impregnation Studies for the Process Modeling/Analysis of Complex Engineering Structures Manufactured by Resin Transfer Molding, *Polymer Composites*, 19(5): 527-542.
- [14] Sun, X.D., Li, S.J. and Lee, L.J. (1998). Mold Filling Analysis in Vacuum-Assisted Resin Transfer Molding. Part I: SCRIMP Based on a High-Permeable Medium, *Polymer Composites*, 19(6): 807-817.
- [15] Ni, J., Li, S.J., Sun, X.D. and Lee, L.J. (1998). Mold Filling Analysis in Vacuum-Assisted Resin Transfer Molding. Part II: SCRIMP Based on Grooves, *Polymer Composites*, 19(6): 818-829.
- [16] Tari, M.J., Imbert, J.P., Lin, M.Y., Lavine, A.S. and Hahn, H.T. (1998). Analysis of Resin Transfer Molding with High Permeability Layers, *Transactions of the ASME, Journal of Manufacturing Science and Engineering*, 120(3): 609-616.
- [17] Hsiao, K.T., Mathur, R. and Advani, S.G. (2000). A Closed Form Solution for Flow During the Vacuum Assisted Resin Transfer Molding Process, *Transactions of the ASME, Journal of Manufacturing Science and Engineering*, 122(3): 463-475.
- [18] Han, K., Jiang, S.L., Zhang, C. and Wang, B. (2000). Flow Modeling and Simulation of SCRIMP for Composite Manufacturing, *Composites Part A*, 31(1): 79-86.

- [19] Chen, R.L., Dong, C.S., Liang, Z.Y., Zhang, C. and Wang, B. (2004). Flow Modeling and Simulation for Vacuum Assisted Resin Transfer Molding Process with the Equivalent Permeability Method, *Polymer Composites*, 25(2): 146-164.
- [20] D'Arcy H. (1856). *Les Fontaines Publiques de la villa de Dijon*. Dalmont, Paris.

Author's Biography

Chensong Dong is a Process Engineer at Rakon, Ltd, New Zealand. He received his Ph.D. in industrial engineering from the Florida State University in 2003. He also holds a B.S. (1994) and an M.S. (1997) in precision instrument engineering from Tianjin University, China. His research interests include: product development, manufacturing process, quartz crystal processing, liquid composite processing and precision metrology. He is the author or coauthor of 30 technical articles.

Contact:

Chensong (Jonathan) Dong

Rakon, Ltd.

Private Bag 99943, Newmarket

Auckland

New Zealand

Phone: +64 (9) 573-5554 ext 389

Fax: +64 (9) 573-5559

Email: jonathan.d@rakon.co.nz